Lipocalin Q83 Reveals a Dual Ligand Binding Mode with Potential Implications for the Functions of Siderocalins

ARTICLE *in* BIOCHEMISTRY · SEPTEMBER 2011

Impact Factor: 3.02 · DOI: 10.1021/bi201115q · Source: PubMed

7 AUTHORS, INCLUDING:

Nicolas Coudevylle
University of Vienna
33 PUBLICATIONS **260** CITATIONS
SEE PROFILE

Leonhard Geist
University of Vienna
10 PUBLICATIONS **100** CITATIONS
SEE PROFILE

Georg Kontaxis
University of Vienna
46 PUBLICATIONS **1,485** CITATIONS
SEE PROFILE

Robert Konrat
University of Vienna
134 PUBLICATIONS **2,970** CITATIONS
SEE PROFILE

BIOCHEMISTRY
including biophysical chemistry & molecular biology

Article

pubs.acs.org/biochemistry

Lipocalin Q83 Reveals a Dual Ligand Binding Mode with Potential Implications for the Functions of Siderocalins

Nicolas Coudevylle,*[,†] Matthias Hoetzinger,[†] Leonhard Geist,[†] Georg Kontaxis,[†] Markus Hartl,[‡] Klaus Bister,[‡] and Robert Konrat[†]

[†]Department of Structural and Computational Biology, Max F. Perutz Laboratories, University of Vienna, Campus Vienna Biocenter 5/1, 1030 Vienna, Austria

[‡]Institute of Biochemistry, Center for Molecular Biosciences (CMBI), University of Innsbruck, Peter-Mayr-Strasse 1a, 6020 Innsbruck, Austria

Supporting Information

ABSTRACT: Siderocalins are particular lipocalins that participate in the innate immune response by interfering with bacterial siderophore-mediated iron uptake. Additionally, siderocalins are involved in several physiological and pathological processes such as inflammation, iron delivery, tissue differentiation, and cancer progression. Here we show that siderocalin Q83 displays an unexpected dual ligand binding mode as it can bind enterobactin and unsaturated fatty acids simultaneously. The solution structure of the siderocalin Q83 in complex with arachidonic acid and enterobactin reveals molecular details of this novel dual binding mode and the determinants of fatty acid binding specificity. Our results suggest that Q83 is a metabolic hub linking iron and fatty acid pathways. This unexpected coupling might contribute to the pleiotropic functions of siderocalins.

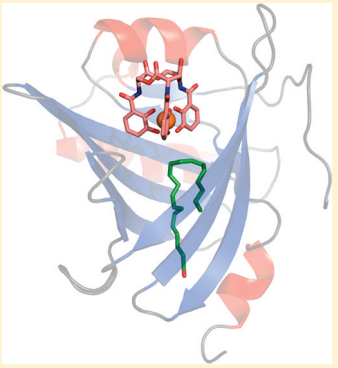

Siderocalins (Scn) are members of the lipocalin family of small secreted proteins characterized by a conserved fold that consists of a β-barrel forming a hydrophobic cavity called "calyx". Lipocalins bind small hydrophobic ligands in their calyx[1] and are involved in many physiological processes such as pheromone transport, cell homeostasis, or prostaglandin synthesis.[2,3] Scns have the distinctive feature to transport ferric iron (FeIII) via catechol-type iron chelators.[4−6] NGAL, the first Scn identified, binds the bacterial siderophore enterobactin with high affinity (K_D = 0.4 nM).[6] Along this line, NGAL is involved in the innate immune response by interfering with microbial siderophore-mediated iron uptake.[7−9] It has recently been reported that NGAL can bind iron without the help of bacterial siderophores but together with small iron chelating metabolites such as catechol or dihydroxybenzoic acid.[4,5] Using these mammalian siderophores, NGAL can be involved in specific iron delivery pathways active during organogenesis and cell differentiation.[10,11] In addition to the well-established iron binding properties of Scns, increasing evidence suggests that siderocalins are also involved in cancer progression[12] and metastasis[13] and contribute to proinflammatory effects,[14,15] although it is not clear how the iron binding properties of Scn are related to these effects.

We have recently shown that quail lipocalin Q83 is a siderocalin.[16] Q83 is highly overexpressed in embryonic fibroblasts transformed by the *v-myc* oncogene,[17] and its chicken homologue (Ch21) is specifically expressed in embryonic tissue.[18,19] These observations are in line with the upregulation of NGAL in tumorigenesis and in organogenesis. Similarly to NGAL, Ch21 is upregulated upon inflammation. Interestingly, Ch21 was shown to bind lipids, preferentially long-chain unsaturated fatty acids like arachidonic acid.[20] Moreover, the gene encoding for Ch21 is clustered on chromosome 17 with two other genes encoding for chondrogenesis associated lipocalins (CAL) CALβ and CALγ.[21,22] All three genes are highly activated during tissue differentiation and inflammation. On the basis of sequence comparison, CALβ presumably binds unsaturated fatty acids, whereas CALγ shows strong homology with the human lipocalin-type prostaglandin synthase. This suggests that Ch21, CALβ, and CALγ are involved in the transport and metabolism of unsaturated fatty acids with possible implications in tissue differentiation and inflammation. If the established siderocalin Q83 shares the same fatty acid binding properties as Ch21, this could lead to important biological implications with respect to the pleiotropic functions of Scns. More specifically, this could explain why Scns show so versatile functions and how Scns are involved in inflammation. We show here that Q83 has indeed dual binding potential, as a siderocalin and a fatty acid binding protein (FABP).

Received: July 19, 2011
Revised: September 27, 2011
Published: September 27, 2011

EXPERIMENTAL PROCEDURES

Expression and Purification of Recombinant Lipocalin Q83. Quail recombinant lipocalin Q83 (157 amino acids) was expressed and purified as described before.[16,17] Q83 mutants (R6A, T90A, and Y92F) were obtained using the QuickChange mutagenesis kit from Stratagene; the primers used are listed in Supporting Information Table 2.

Ligand Preparation. Metal-free enterobactin as well as $[Fe^{III}(Ent)]^{3-}$ and $[Ga^{III}(Ent)]^{3-}$ was obtained as described previously.[16] Lipids were purchased from Sigma-Aldrich.

DAUDA Replacement Experiments. Fluorescence was measured on a Perkin-Elmer LS 50B fluorimeter with 5 nm slit band-pass using the characteristic DAUDA excitation (λ_{exc} = 350 nm) and emission (λ_{em} = 490 nm) wavelengths. Measurements were made at a protein concentration of 2 μM in 20 mM NaP_i, 50 mM NaCl, 0.5 mM DTT, pH 6.5 at 25 °C. The volume of the cell was 2 mL. The change of fluorescence intensity was followed upon addition of a concentrated ligand solution (200 μM in DMSO). Loading of DAUDA to Q83 was fitted using QtiPlot assuming a single binding site model [23] using the following equation:

$$I = I_{max} \times ([Pt] + [Lt] + K_D - (([P] + [L] + K_D)^2 - 4[P][L])^{1/2})/2[P]$$

where $[P]$, $[L]$, K_D, and I_{max} are the protein concentration, DAUDA concentration, dissociation constant, and the intensity at saturating concentration of DAUDA, respectively. For the DAUDA replacement experiments,[24] the decrease of fluorescence intensity against the natural logarithm of the lipid concentration was fitted to a logistic function using QtiPlot. At the inflection point, half of the protein sites are replaced by the lipid. The lipid concentration at that point was used to calculate the dissociation constant of Q83 for the lipid using the following relation:

$$K_D^{Lipid} = \frac{[Lipid]}{1 + \frac{[DAUDA]}{K_D^{DAUDA}}}$$

NMR Spectroscopy. All NMR samples were concentrated up to 0.5 mM of protein in 20 mM NaPi, 50 mM NaCl, 0.5 mM DTT, pH 6.5 supplemented with 10% D_2O. NMR experiments were carried out at 25 °C on Varian Inova spectrometers operating at 500, 600, or 800 MHz. All spectra were processed using NMRPipe/NMRDraw[25] and analyzed with Sparky and CARA.[26] Residual dipolar couplings (RDC) were measured on a partially aligned sample using bacteriophage Pf1 (Profos) at a concentration of 15 mg/mL with 150 mM NaCl. One bond, $^1J_{1H,15N}$ and $^1D_{1H,15N}$, were measured on ^1H,^{15}N HSQC spectra acquired using the in-phase/antiphase (IPAP) method.[27]

Resonance Assignment of the Q83/$[Ga^{III}(Ent)]^{3-}$/AA Complex. Backbone amide $^1H^N$, ^{15}N, $^{13}C^{\alpha}$, $^{13}C'$, and side chain $^{13}C^{\beta}$ resonances of the Q83/$[Ga^{III}(Ent)]^{3-}$/AA complex were assigned using $^1H-^{15}N$ HSQC, HNCO, HN(CA)CO, HNCA, HN(CO)CA, HNCACB, and CBCA(CO)NH experiments. Backbone H^{α}, aliphatic side chain protons, and carbons resonances were assigned via HCCH-TOCSY and $^{15}N/^{13}C$-HSQC-NOESY experiments. Resonances of the ligands in the bound state were assigned as previously described[16] using a 2D $^{13}C-^{15}N$ filtered $^1H-^1H$ NOESY experiment using an adiabatic ^{13}C inversion pulse in the editing delays.[28] Chemical shifts were deposited in the BioMagResBank (BMRB) under the accession number 17577.

Solution Structure of the Q83/$[Ga^{III}(Ent)]^{3-}$/AA Complex. The structure of the protein alone was first solved in the bound state. Backbone φ and ψ dihedral restraints were derived from the program TALOS[29] using as input the ^1H, ^{13}C, and ^{15}N backbone chemical shifts. Only TALOS predictions with 10/10 agreeing matches were converted into a torsion angle restraint. Dihedral restraints, $^1H-^{13}C/^{15}N$ HSQC-NOESY spectra, and ^1H, ^{13}C, and ^{15}N chemical shifts were used as input for the ATNOS/CANDID package[30,31] to generate a first ensemble of structures. This early ensemble was used to manually finalize the assignment of the $^1H-^{13}C/^{15}N$ HSQC-NOESY spectra. Dihedral angles and distance restraints were then used in a MD protocol of Xplor-NIH[32] to generate an ensemble of 100 structures of lipocalin Q83 in the $[Ga^{III}(Ent)]^{3-}$/AA-bound state.

Enterobactin starting coordinates were taken from the crystal structure of vanadium enterobactin,[33] and AA starting coordinates were taken from the Protein Data Bank (PDB). The parameters of the ligands were calculated using the PRODRG server.[34] The ligands were docked into the structure by using intermolecular distance restraints obtained from (i) a 2D $^{15}N-^{13}C$ double filtered $^1H-^1H$ NOESY experiment;[16] (ii) ω_1-[^{13}C]-filtered 3D $^1H-^{13}C$ NOESY-HSQC.[35] For the enterobactin ligand, only unambiguous restraints were used (Supporting Information Table 1). For the AA ligand, a combination of ambiguous and unambiguous restraints was defined as follows: the most upfield AA resonance has been assigned to the methyl moiety of the ligand; AA resonances from 0 to 4 ppm were ambiguously assigned to methylenic protons; AA resonances from 4 to 6 ppm were ambiguously assigned to olefinic protons (Supporting Information Table 1). $[Ga^{III}(Ent)]^{3-}$ was docked first to Q83, and AA was subsequently docked to the Q83/$[Ga^{III}(Ent)]^{3-}$ complex. In both cases, the ligand was first placed 50 Å away from the protein. A first step of rigid body minimization allowed the correct positioning of the ligand with respect to the protein. A second step of simulated annealing followed by a short energy minimization led to a final ensemble of 200 structures of the complex.

After docking with both ligands, the 50 structures of the Q83/$[Ga^{III}(Ent)]^{3-}$/AA complex with the lowest energy were selected for a final RDC refinement protocol performed with Xplor-NIH and the protein-2.0 force field. The 20 structures with the lowest energy were selected as the final ensemble of structures describing the Q83/$[Ga^{III}(Ent)]^{3-}$/AA complex in solution and deposited in the Protein Data Bank under the accession number 2LBV. Experimental restraints and structural statistics are summarized in Table 2. The lowest energy structure from the final ensemble was considered as the most representative of the ensemble and was used for preparing the figures.

RESULTS

Lipocalin Q83 Binds Unsaturated Fatty Acids in a Secondary Binding Site with Nanomolar Affinity. Ch21, the chicken homologue of Q83, has been shown to bind unsaturated fatty acids with nanomolar affinity.[20] Considering the high sequence identity (87%) between Ch21 and Q83, it is reasonable to assume that Q83 binds fatty acids. In order to probe a possible interaction between Q83 and unsaturated fatty

acids, $^{1}H-^{15}N$ HSQC-based titrations of Q83 with different fatty acids were carried out. Since Ch21 preferentially binds arachidonic acid (AA; C20:4 *cis-,cis-,cis-,cis*-5,8,11,14), Q83 binding to AA was tested first. Upon addition of AA, the emergence of a second subset of resonances is observed in the $^{1}H-^{15}N$ HSQC spectrum, followed by the concomitant disappearance of the original set of resonances, indicating that Q83 binds AA with high affinity (slow exchange regime on the NMR time scale). ^{1}H, ^{15}N, and ^{13}C resonances of the Q83/AA complex were assigned by conventional three-dimensional heteronuclear experiments. By comparing the amide chemical shifts (^{15}N and ^{1}H) of each residue in the free and AA-bound form and mapping them onto the 3D structure, we were able to identify the AA binding site, which is located at the closed end of the calyx (Figure 1A). The localization of the AA binding site differs significantly from the classical lipocalin ligand binding site. Indeed, Q83 binds enterobactin at the hydrophilic open end of the β-barrel [16] (Figure 1B), leading to tryptophan fluorescence quenching. In contrast, AA seems to bind in the more hydrophobic environment formed by the narrow end of the calyx. The hydrophobicity of the AA binding site is also reflected by the fact that Trp_{13} (located in this part of the protein) does not contribute to the endogenous fluorescence of Q83 (as enterobactin binding to the hydrophilic calyx leads to a nearly complete fluorescence quenching). Therefore, AA binding does not lead to fluorescence quenching despite the presence of Trp_{13} at the AA binding site (data not shown).

In order to measure the affinity of Q83 for AA, and given that AA binding does not lead to fluorescence quenching, a DAUDA (11-[5-(dimethylamino)-1-naphthalenesulfonylamino]-undecanoic acid) replacement experiment was carried out.[36] DAUDA has been chosen because of its chemical similarity with AA. Upon excitation at 350 nm, addition of DAUDA to Q83 led to an increasing emission peak at 490 nm. By itself, this observation already confirms that Q83 contains an apolar binding site. Saturation of Q83 by DAUDA was

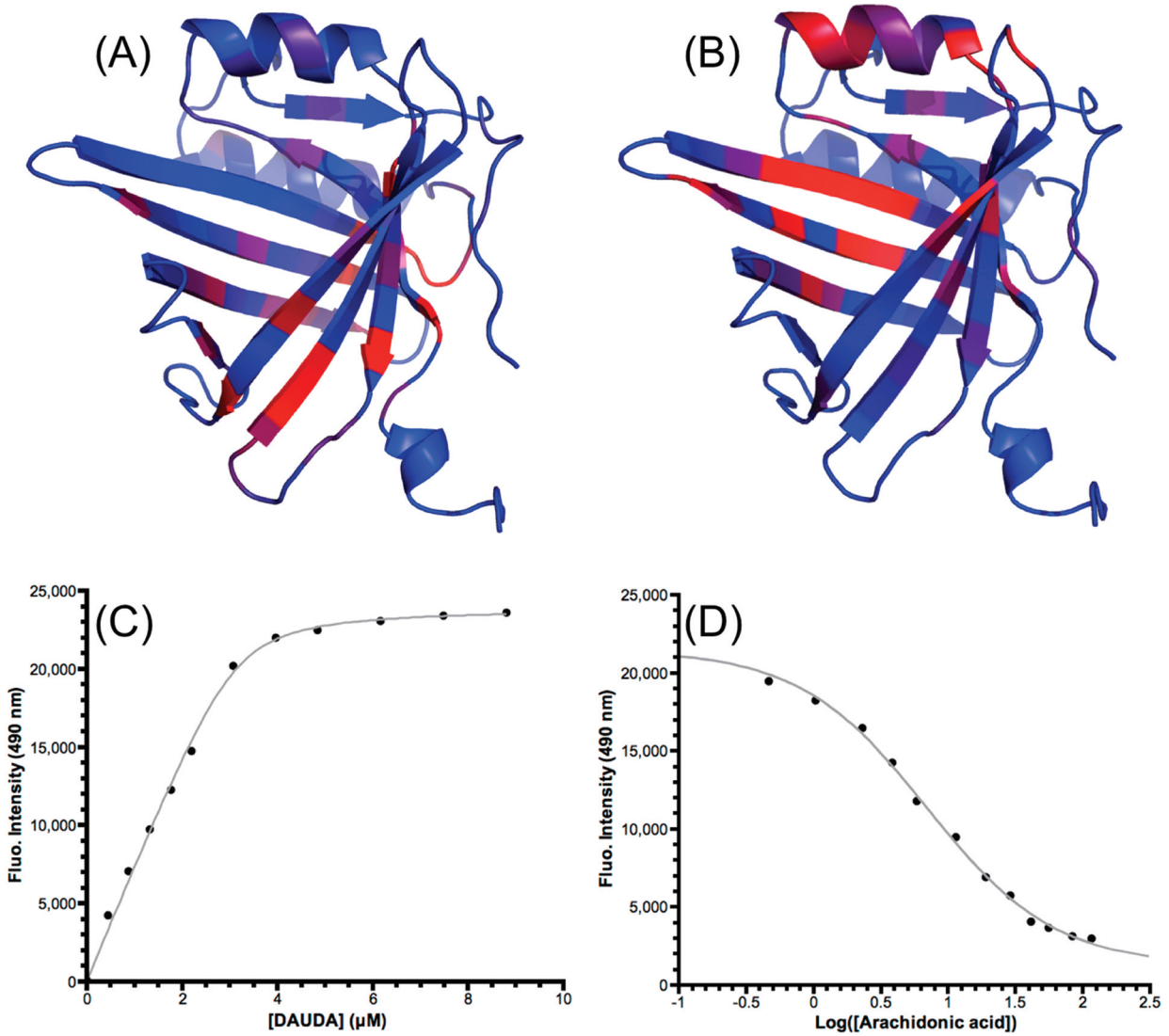

Figure 1. Siderocalin Q83 binds arachidonic acid in an unexpected binding site. (A) Amide chemical shift perturbation upon AA binding. Significant chemical shift changes are highlighted as a blue (no perturbation) to red (highest perturbation) color gradient on the solution structure of free Q83 (PDB accession code 1JZU). (B) Amide chemical shift perturbation upon $[Ga^{III}(Ent)]^{3-}$ binding.[16] (C) Increase of DAUDA fluorescence upon binding to Q83. Upon excitation at 350 nm, addition of DAUDA to Q83 leads to an increasing emission peak at 490 nm. The normalized fluorescence intensity is plotted as a function of DAUDA concentration. (D) DAUDA fluorescence quenching assay. Subsequent addition of AA to the Q83/DAUDA complex quenched the 490 nm emission. The normalized fluorescence intensity is plotted as a function of AA concentration.

dx.doi.org/10.1021/bi201115q | *Biochemistry* 2011, 50, 9192–9199

achieved, allowing the calculation of the Q83/DAUDA complex dissociation constant: 0.104 μM (Figure 1C). Subsequent addition of AA to the Q83/DAUDA complex quenched the 490 nm emission, clearly showing that AA replaces DAUDA from Q83. Fitting of the 490 nm quenching upon AA addition revealed a dissociation constant (K_D) of the Q83/AA complex of 26 nM (Figure 1D). The affinity of Q83 for other fatty acids was measured following the same procedure (Table 1). Overall, the affinity range measured for

Table 1. Affinity of Lipocalin Q83 for Different Fatty Acids

Q83 form	ligand	K_D (nM)
WT	DAUDA	104
	arachidonic acid	26
	oleic acid	44
	linoleic acid	43
	palmitic acid	77
	myristic acid	103
	lauric acid	200
R6A	DAUDA	120
	arachidonic acid	98
T90A	DAUDA	890
	arachidonic acid	276
Y92F	DAUDA	265
	arachidonic acid	1864

Q83 is of the same order as that determined for Ch21[20] as well as for other FABPs.[37,38] AA binds with the highest affinity, and reduction of the aliphatic chain from 20 to 18 C atoms reduces the affinity by a factor of about 2, from a K_D of 26 nM for AA to 43 nM for linoleic acid (C18:2 *cis*-,*cis*-9−12) and 44 nM for oleic acid (C18:1 *cis*-9). Reduction of the number of double bonds does not seem to affect the affinity because almost identical values were obtained for linoleic and oleic acid. Further shortening of the aliphatic chain decreases the affinity even further, from a K_D of 77 nM for palmitic acid (C16:0), 103 nM for myristic acid (C14:0), and up to 200 nM for lauric acid (C12:0). Overall, the affinity of lipid binding to Q83 is similar to other FABPs. However, the locations of ligand binding sites differ strikingly.

Lipocalin Q83 Can Simultaneously Bind Enterobactin and Unsaturated Fatty Acids. Because the Q83 enterobactin and AA binding sites do not overlap, it could be inferred that Q83 has the ability to bind both ligands simultaneously. In order to investigate this possibility, ^{1}H−^{15}N HSQC spectra of Q83 were recorded before (Figure 2A) and after addition of ligand (AA or $[Ga^{III}(Ent)]^{3-}$). As expected, the spectrum of the AA-bound form clearly differs from the $[Ga^{III}(Ent)]^{3-}$-bound form (Figure 2B,). Another set of spectra was recorded after addition of the complementary ligand. Both samples exhibit the same ^{1}H−^{15}N HSQC spectra which differ from both the Q83/$[Ga^{III}(Ent)]^{3-}$ and the Q83/AA spectra (Figure 2D). This demonstrates that Q83 can bind both ligands simultaneously to form a unique Q83/$[Ga^{III}(Ent)]^{3-}$/AA ternary complex, regardless of the sequence of ligand binding reactions.

If Q83 is able to bind $[Fe^{III}(Ent)]^{3-}$ and AA simultaneously, the question naturally arises whether the binding of one ligand affects the binding of the other. The affinity of Q83/AA (i.e., in presence of saturating AA concentration) for $[Fe^{III}(Ent)]^{3-}$ has been measured by tryptophan fluorescence quenching and led to a dissociation constant (K_D) of 1.3 nM. Therefore, the

Table 2. NMR and Refinement Statistics for the Q83/$[Ga^{III}(Ent)]^{3-}$/AA Complex

NMR geometric restraints	
total distance restraints	1299
intraresidue	189
inter-residue	1007
sequential ($\|i - j\| = 1$)	484
medium-range ($\|i - j\| \leq 4$)	145
long-range ($\|i - j\| \geq 5$)	378
Q83-$[Ga^{III}(Ent)]^{3-}$ intermolecular restraints	21
unambigous Q83−AA intermolecular restraints	9
ambigous Q83−AA intermolecular restraints	6
hydrogen bonds[a]	64
Ga^{3+}−enterobactin restraints[b]	6
total dihedral restraints	230
φ	115
ψ	115
total $^1D_{^1H-^{15}N}$ residual dipolar couplings	123
structure statistics	
violations (rmsd and sd)	
distance restraints	0.015 ± 0.001
dihedral restraints	2.37 ± 0.3
$^1D_{^1H-^{15}N}$ RDC	0.90 ± 0.07
deviation from idealized geometry	
bond lengths (Å)	0.0040 ± 0.003
bond angles (°)	0.7 ± 0.02
Ramachandran statistics[c]	
residues in most favored regions	86%
residues in additional allowed regions	13%
residues in generously allowed regions	1%
residues in disallowed regions	0%
average rms deviation (Å)	
heavy atoms (12−155)	1.74 ± 0.42
backbone atoms (12−155)	0.84 ± 0.20

[a]Two restraints for each hydrogen bond were included in the calculations ($d_{HN-O} \leq 2.5$ Å and $d_{N-O} \leq 3.5$ Å). [b]The Ga^{3+}−O distance restraints were restrained to 1.8−2.0 Å. [c]Ramachadran statistics were obtained using the PROCHECK NMR software.

binding of AA to Q83 seems to provoke only a slight decrease in affinity of Q83 for $[Fe^{III}(Ent)]^{3-}$ (from a K_D of 0.5 to 1.3 nM). However, the reciprocal experiment (measuring the affinity of Q83/$[Fe^{III}(Ent)]^{3-}$ for AA) could not be realized since the binding of $[Fe^{III}(Ent)]^{3-}$ hampers the binding of DAUDA, suggesting that the DAUDA binding site overlaps with both the AA and $[Fe^{III}(Ent)]^{3-}$ binding sites.

Solution Structure of the Q83/$[Ga^{III}(Ent)]^{3-}$/AA Complex. In order to gain further insight into the binding mode of Q83 for AA and to understand how this protein accommodates two ligands simultaneously, the solution structure of the ternary Q83/$[Ga^{III}(Ent)]^{3-}$/AA complex was solved by NMR. During the calculation, the protein in its bound state was treated first. The ligands were subsequently added to the calculation, first $[Ga^{III}(Ent)]^{3-}$ based on 21 unambiguous intermolecular distance restraints followed by AA, based on 9 unambiguous and 6 ambiguous intermolecular distance restraints (Supporting Information Table 1). The resulting complex structure was subjected to a final RDC refinement procedure. The 20 final structures of the Q83/$[Ga^{III}(Ent)]^{3-}$/AA complex exhibit a pairwise atomic rms distribution about the mean coordinate positions of 0.84 ± 0.20 Å for the backbone atoms and 1.74 ± 0.42 Å for all heavy atoms from residues Lys_{12} to Asp_{155} of the 157 amino acid recombinant Q83 protein. The N- and

dx.doi.org/10.1021/bi201115q | *Biochemistry* 2011, 50, 9192−9199

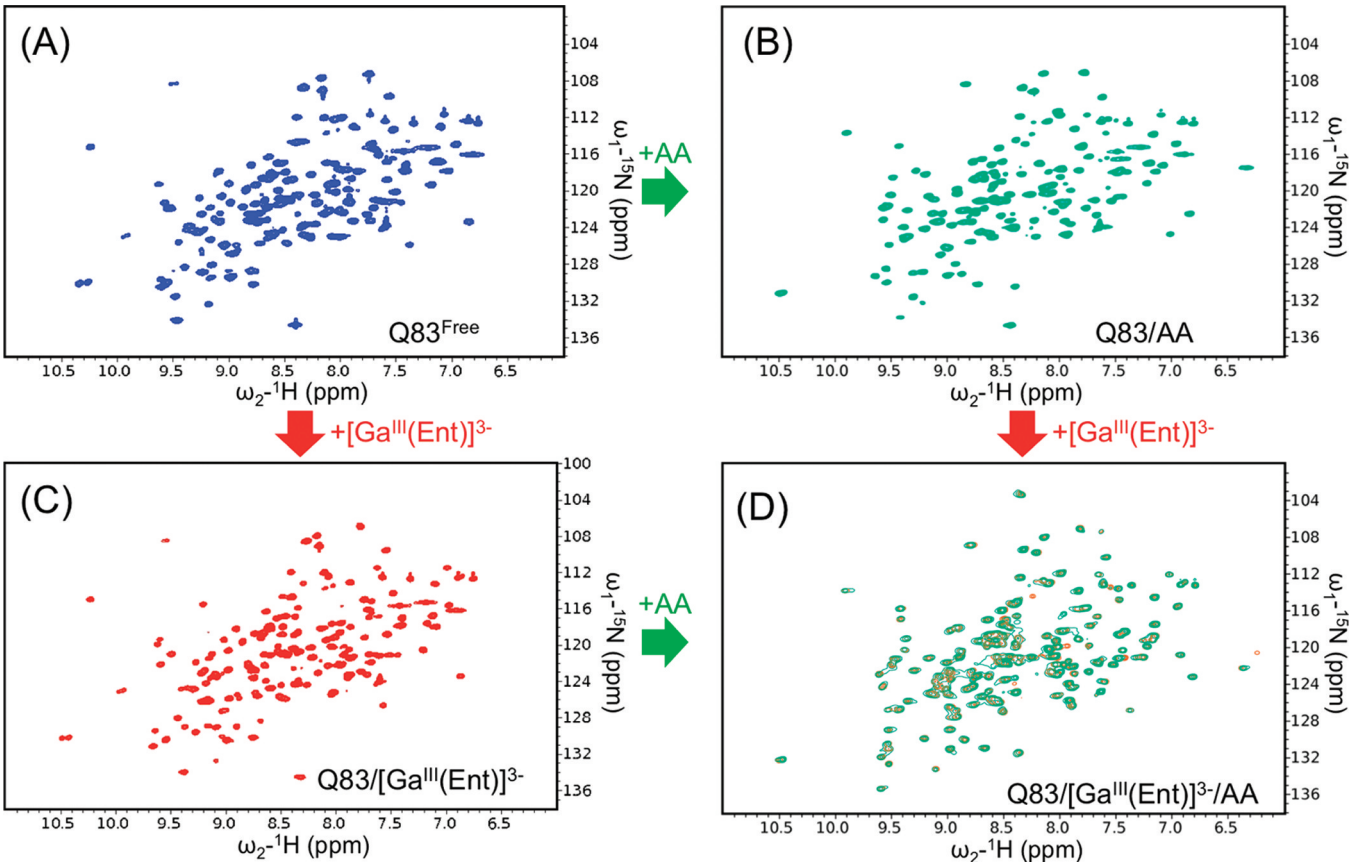

Figure 2. Q83 binds Enterobactin and AA simultaneously to form a unique ternary complex. (A) $^{1}H-^{15}N$ HSQC spectrum of Q83. (B) $^{1}H-^{15}N$ HSQC spectrum of the Q83/AA complex. (C) $^{1}H-^{15}N$ HSQC spectrum of Q83/$[Ga^{III}(Ent)]^{3-}$ complex. (D) Overlay of the $^{1}H-^{15}N$ HSQC spectra of the Q83/$[Ga^{III}(Ent)]^{3-}$/AA and Q83/AA/$[Ga^{III}(Ent)]^{3-}$ complexes (red and green resonances, respectively).

C-termini appeared to be less well-defined (Figure 3A). In the final structure ensemble, all of the backbone torsion angles of the non-glycine residues fall in the allowed regions of the Ramachandran plot (Table 2). In the Q83/$[Ga^{III}(Ent)]^{3-}$/AA complex, Q83 retains its classical lipocalin fold. As expected, the enterobactin ligand binds in the open end of the β-barrel while the AA ligand is embedded in the hydrophobic environment formed by the narrow end of the barrel. The location and the conformation of the AA ligand through the final ensemble are rather well-defined (Figure 3B). In all conformers, AA adopts the classical "U-shape" commonly found with FABPs.[38] Both the methyl and carboxylate moieties are pointing toward the closed end of the calyx, whereas most double bonds are close to the enterobactin binding site (Figure 3C,D). The fold of Q83 and the position of the enterobactin ligand do not seem to be affected by the binding of AA since the Q83/$[Ga^{III}(Ent)]^{3-}$/AA complex superimposes nicely onto the $[Ga^{III}(Ent)]^{3-}$-bound forms with an rmsd of 1.1 Å (Figure 4A). Only the interstrand loops at the narrow end of the calyx (i.e., the AA binding site) exhibit significant conformational changes (Figure 4B). Specifically, the loops β_3-β_4, β_5-β_6, and β_7-β_8 as well as the helix α_1 appear to accommodate AA by bending toward the ligand, probably in order to strengthen the interaction with the ligand by limiting contacts with the bulk water and potentially acting as a lid.

Arachidonic Acid Binding Mode. The Q83/AA interaction appears to be stabilized by numerous hydrophobic contacts between the aliphatic chain of the lipid and aromatic residues of the protein. Moreover, the carboxylate group of the lipid interacts with the side chains of residues Thr_{90} and Tyr_{92} (Figure 4C) presumably via direct or water-mediated hydrogen bonds. A similar mode of interaction is observed for other types of FABPs.[38] For these proteins, the carboxylate moiety of AA is often found to be engaged in hydrogen bonds with a tyrosine hydroxyl and a serine or threonine hydroxyl. In addition, an arginine residue is frequently present, forming a salt bridge or contributing to the hydrogen bond network stabilizing the AA carboxylate moiety. The AA binding mode of Q83 looks very similar, at least concerning the involvement of a tyrosine and a threonine residue, suggesting a conservation of this canonical lipid binding mode. Additionally, an arginine residue is also found in the neighborhood of the carboxylate (Arg_6 on helix α_1), but the conformation of this residue is rather ill defined within the structural ensemble. In order to evaluate the importance of these residues for AA binding, specific Q83 mutants were designed and their affinity for AA was measured (Table 1). When compared to the wild-type (K_D 26 nM), the affinity of the mutants for AA is reduced by a factor of 4 for R6A (K_D 98 nM), a factor of 10 for T90A (K_D 276 nM), and a factor of 72 for Y92F (K_D 1864 nM). This clearly indicates that Thr_{90} and especially Tyr_{92} are actively involved in AA binding.

DISCUSSION

We report here that Q83, a lipocalin of the siderocalin class, binds unsaturated fatty acids with nanomolar affinity. Overall, the fatty acid binding properties of Q83 are similar to those of other FABPs in terms of affinity and binding mode, but the location of the ligand binding site in Q83 considerably differs

dx.doi.org/10.1021/bi201115q | Biochemistry 2011, 50, 9192–9199

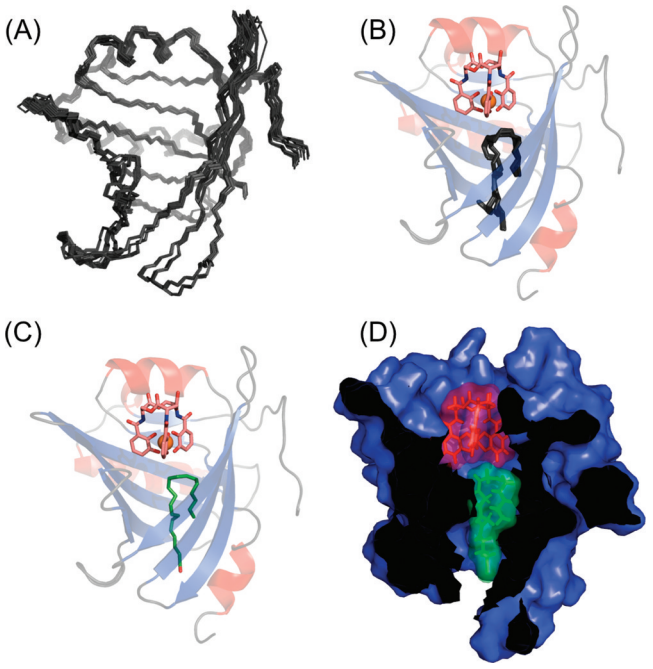

Figure 3. Solution structure of the Q83/$[Ga^{III}(Ent)]^{3-}$/AA complex. (A) Backbone superimposition of the final set of 20 structures for the Q83/$[Ga^{III}(Ent)]^{3-}$/AA complex. (B) AA distribution within the Q83 calyx. The ribbon model of the most representative complex is rendered transparent; AA molecules are depicted as black sticks. (C) Representative ribbon model of the Q83/$[Ga^{III}(Ent)]^{3-}$/AA complex. The protein ribbon is rendered transparent; enterobactin is represented with pink sticks, and Ga(III) is depicted as an orange sphere and AA with green sticks. (D) Cutaway surface representation of the Q83/$[Ga^{III}(Ent)]^{3-}$/AA complex; the protein surface is colored in blue, and the $[Ga^{III}(Ent)]^{3-}$ and AA are rendered transparent and colored in red and green, respectively.

from the canonical lipocalin binding site. Most importantly, Q83 is able to bind both enterobactin and AA simultaneously. To the best of our knowledge, such dual binding potential is a unique feature for a lipocalin. Some lipocalins are able to bind two different ligands, such as the lipocalin-type prostaglandin D synthase,[39] the human apolipoprotein D,[40] or the tick histamine binding proteins,[41] but the ligands either are of the same chemical nature or bind both to the calyx and therefore cannot bind simultaneously. The striking features of Q83, that is, unusual binding site and the ability of binding two unrelated ligands simultaneously, make it a unique member of the lipocalin family.

Interestingly, the key residues involved in fatty acid binding (Thr_{90} and Tyr_{92}) are conserved in NGAL, in the putative siderocalin LCN12 [42] (Figure 4D), and many other lipocalins. Consequently, the fatty acid binding properties of Q83 could be found in other lipocalins and siderocalins. Siderocalins have been shown to exhibit pleiotropic functions from iron delivery to inflammation and cancer progression. Our finding that siderocalin Q83 also binds unsaturated fatty acids opens a whole new range of possibilities to explain the multiple functions of siderocalins. Indeed, unsaturated fatty acids are the precursors of prostaglandins and leukotrienes, two mediators of inflammation. Consequently, the active involvement of Q83/Ch21 during inflammation in conjunction with CALβ and CALγ is very likely to be related to Q83/Ch21 fatty acid binding properties.

Nevertheless, the exact function of Q83 and by extension of other siderocalins during inflammation remains to be determined. Q83 could act as a simple fatty acid carrier during inflammation, independent of its iron binding properties. In such a case, Q83 would act as either a fatty acid carrier, iron transporter, or bacteriostatic, depending on the physiological context. Another, more seducing, possibility is that Q83 could carry and/or provoke synergic physiological effects of iron and AA during inflammation. Indeed, the metabolism of iron and unsaturated fatty acids are intimately linked, as many enzymes involved in the synthesis of prostaglandins and leukotrienes are using iron as a cofactor, such as lipooxygenases,

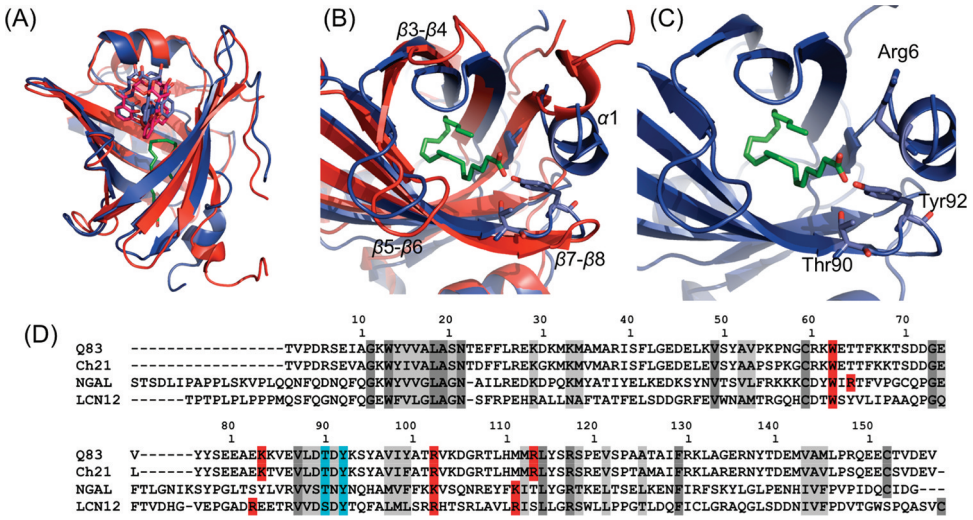

Figure 4. Structural comparison and AA binding mode. (A) Backbone superimposition of the solution structures of the Q83/$[Ga^{III}(Ent)]^{3-}$ (in red) and the Q83/$[Ga^{III}(Ent)]^{3-}$/AA (in blue) complexes. (B) Structural comparison of the AA binding site in the Q83/$[Ga^{III}(Ent)]^{3-}$ (in red) and the Q83/$[Ga^{III}(Ent)]^{3-}$/AA (in blue) complexes. AA is depicted with green sticks. (C) Structural details of the AA binding site. Residues involved in AA binding are depicted as blue sticks. (D) Sequence alignment of the secreted forms of putative and experimentally proven siderocalins with NGAL; Q83, quail siderocalin Q83; Ch21, chicken lipocalin Ch21; NGAL, human NGAL; LCN12, human lipocalin 12, isoform a. Conserved and homologous residues are highlighted in dark and light gray, respectively, residues involved in siderophore binding are highlighted in red, and residues involved in AA binding are highlighted in blue.

dx.doi.org/10.1021/bi201115q | *Biochemistry* 2011, 50, 9192–9199

cyclooxygenases, and monooxygenases. Since mammalian siderophores have recently been identified, these synergistic effects could take place in the absence of bacterial infection. In summary, our finding that Q83 binds AA and enterobactin simultaneously suggests that the Q83 siderocalin is a metabolic hub linking iron and fatty acid pathways. This unexpected coupling of important physiological pathways might contribute to pleiotropic functions of siderocalin.

■ ASSOCIATED CONTENT

Ⓢ Supporting Information

Tables S1 and S2. This material is available free of charge via the Internet at http://pubs.acs.org.

■ AUTHOR INFORMATION

Corresponding Author

*Phone: +00 43 1 427752227. Fax: +00 43 1 42779522. E-mail: nicolas.coudevylle@univie.ac.at.

Funding

This work was supported by Austrian Science Fund (FWF) grants P20549-N19, P22125-B12, P17041, and P18148. N.C. is a recipient of a Lise Meitner FWF fellowship.

■ ABBREVIATIONS

(DAUDA), 11-[5-(dimethylamino)-1-naphthalenesulfonylamino]-undecanoic acid; (AA), arachidonic acid; (CAL), chondrogenesis associated lipocalin; (DMSO), dimethyl sulfoxide; (DTT), dithiothreitol; (FABP), fatty acid binding protein; (HSQC), heteronuclear single quantum correlation; (LCN12), human lipocalin 12; (MD), molecular dynamic; (NGAL), neutrophil gelatinase associated lipocalin; (NMR), nuclear magnetic resonance; (NOE), nuclear Overhauser effect; (RDC), residual dipolar couplings; (rmsd), root mean squared deviation; (Scn), siderocalin

■ REFERENCES

(1) Flower, D. R., North, A. C., and Sansom, C. E. (2000) The lipocalin protein family: structural and sequence overview. *Biochim. Biophys. Acta 1482*, 9−24.

(2) Flower, D. R. (1994) The lipocalin protein family: a role in cell regulation. *FEBS Lett. 354*, 7−11.

(3) Flower, D. R. (1996) The lipocalin protein family: structure and function. *Biochem. J. 318*, 1−14.

(4) Bao, G., Clifton, M., Hoette, T. M., Mori, K., Deng, S. X., Qiu, A., Viltard, M., Williams, D., Paragas, N., Leete, T., Kulkarni, R., Li, X., Lee, B., Kalandadze, A., Ratner, A. J., Pizarro, J. C., Schmidt-Ott, K. M., Landry, D. W., Raymond, K. N., Strong, R. K., and Barasch, J. (2010) Iron traffics in circulation bound to a siderocalin (NGAL)−catechol complex. *Nat. Chem. Biol. 6*, 602−609.

(5) Devireddy, L. R., Hart, D. O., Goetz, D. H., and Green, M. R. (2010) A mammalian siderophore synthesized by an enzyme with a bacterial homolog involved in enterobactin production. *Cell 141*, 1006−1017.

(6) Goetz, D. H., Holmes, M. A., Borregaard, N., Bluhm, M. E., Raymond, K. N., and Strong, R. K. (2002) The neutrophil lipocalin NGAL is a bacteriostatic agent that interferes with siderophore-mediated iron acquisition. *Mol. Cell 10*, 1033−1043.

(7) Berger, T., Togawa, A., Duncan, G. S., Elia, A. J., You-Ten, A., Wakeham, A., Fong, H. E., Cheung, C. C., and Mak, T. W. (2006) Lipocalin 2-deficient mice exhibit increased sensitivity to *Escherichia coli* infection but not to ischemia-reperfusion injury. *Proc. Natl. Acad. Sci. U.S.A. 103*, 1834−1839.

(8) Chan, Y. R., Liu, J. S., Pociask, D. A., Zheng, M., Mietzner, T. A., Berger, T., Mak, T. W., Clifton, M. C., Strong, R. K., Ray, P., and Kolls, J. K. (2009) Lipocalin 2 is required for pulmonary host defense against *Klebsiella* infection. *J. Immunol. 182*, 4947−4956.

(9) Flo, T. H., Smith, K. D., Sato, S., Rodriguez, D. J., Holmes, M. A., Strong, R. K., Akira, S., and Aderem, A. (2004) Lipocalin 2 mediates an innate immune response to bacterial infection by sequestrating iron. *Nature 432*, 917−921.

(10) Devireddy, L. R., Gazin, C., Zhu, X., and Green, M. R. (2005) A cell-surface receptor for lipocalin 24p3 selectively mediates apoptosis and iron uptake. *Cell 123*, 1293−1305.

(11) Yang, J., Goetz, D., Li, J. Y., Wang, W., Mori, K., Setlik, D., Du, T., Erdjument-Bromage, H., Tempst, P., Strong, R., and Barasch, J. (2002) An iron delivery pathway mediated by a lipocalin. *Mol. Cell 10*, 1045−1056.

(12) Yang, J., Bielenberg, D. R., Rodig, S. J., Doiron, R., Clifton, M. C., Kung, A. L., Strong, R. K., Zurakowski, D., and Moses, M. A. (2009) Lipocalin 2 promotes breast cancer progression. *Proc. Natl. Acad. Sci. U.S.A. 106*, 3913−3918.

(13) Shi, H, Gu, Y, Yang, J, Xu, L, Mi, W, and W, Y. (2008) Lipocalin 2 promotes lung metastasis of murine breast cancer cells. *J. Exp. Clin. Cancer Res. 77*, 83.

(14) Catalan, V., Gomez-Ambrosi, J., Rodriguez, A., Ramirez, B., Silva, C., Rotellar, F., Gil, M. J., Cienfuegos, J. A., Salvador, J., and Fruhbeck, G. (2009) Increased adipose tissue expression of lipocalin-2 in obesity is related to inflammation and matrix metalloproteinase-2 and metalloproteinase-9 activities in humans. *J. Mol. Med. 87*, 803−813.

(15) Bachman, M. A., Miller, V. L., and Weiser, J. N. (2009) Mucosal lipocalin 2 has pro-inflammatory and iron-sequestering effects in response to bacterial enterobactin. *PLoS Pathog. 5*, e1000622.

(16) Coudevylle, N., Geist, L., Hotzinger, M., Hartl, M., Kontaxis, G., Bister, K., and Konrat, R. (2010) The v-myc-induced Q83 lipocalin is a siderocalin. *J. Biol. Chem. 285*, 41646−41652.

(17) Hartl, M., Matt, T., Schuler, W., Siemeister, G., Kontaxis, G., Kloiber, K., Konrat, R., and Bister, K. (2003) Cell transformation by the v-myc oncogene abrogates c-Myc/Max-mediated suppression of a C/EBP β-dependent lipocalin gene. *J. Mol. Biol. 333*, 33−46.

(18) Descalzi Cancedda, F., Manduca, P., Tacchetti, C., Fossa, P., Quarto, R., and Cancedda, R. (1988) Developmentally regulated synthesis of a low molecular weight protein (Ch21) by differentiating chondrocytes. *J. Cell Biol. 107*, 2455−2463.

(19) Manduca, P., Descalzi Cancedda, F., Tacchetti, C., Quarto, R., Fossa, P., and Cancedda, R. (1989) Synthesis and secretion of Ch 21 protein in embryonic chick skeletal tissues. *Eur. J. Cell Biol. 50*, 154−161.

(20) Cancedda, F. D., Malpeli, M., Gentili, C., Di Marzo, V., Bet, P., Carlevaro, M., Cermelli, S., and Cancedda, R. (1996) The developmentally regulated avian Ch21 lipocalin is an extracellular fatty acid-binding protein. *J. Biol. Chem. 271*, 20163−20169.

(21) Pagano, A., Crooijmans, R., Groenen, M., Randazzo, N., Zerega, B., Cancedda, R., and Dozin, B. (2003) A chondrogenesis-related lipocalin cluster includes a third new gene, CALγ. *Gene 305*, 185−194.

(22) Pagano, A., Giannoni, P., Zambotti, A., Randazzo, N., Zerega, B., Cancedda, R., and Dozin, B. (2002) CALβ, a novel lipocalin associated with chondrogenesis and inflammation. *Eur. J. Cell Biol. 81*, 264−272.

(23) Auguin, D., Barthe, P., Royer, C., Stern, M. H., Noguchi, M., Arold, S. T., and Roumestand, C. (2004) Structural basis for the co-activation of protein kinase B by T-cell leukemia-1 (TCL1) family proto-oncoproteins. *J. Biol. Chem. 279*, 35890−35902.

(24) Bath, J. L., Robinson, M., Kennedy, M. W., Agbasi, C., Linz, L., Maetzold, E., Scheidt, M., Knox, M., Ram, D., Hein, J., Clark, C., and Drees, J. (2009) Identification of a secreted fatty acid and retinol-binding protein (Hp-FAR-1) from *Heligmosomoides polygyrus*. *J. Nemat. 41*, 228−233.

(25) Delaglio, F., Grzesiek, S., Vuister, G. W., Zhu, G., Pfeifer, J., and Bax, A. (1995) NMRPipe: a multidimensional spectral processing system based on UNIX pipes. *J. Biomol. NMR 6*, 277−293.

(26) Keller, R. (2004) *The computer aided resonance assignment tutorial*, Cantina Verlag, Goldau, Switzerland.

(27) Ottiger, M., and Bax, A. (1998) Characterization of magnetically oriented phospholipid micelles for measurement of dipolar couplings in macromolecules. *J. Biomol. NMR 12*, 361−372.
(28) Zwahlen, C., Legault, P., Vincent, S., Greenblatt, J., Konrat, R., and Kay, L. E. (1997) Methods for measurement of intermolecular NOEs by multinuclear NMR spectroscopy: application to a bacteriophage λ N-peptide/boxB RNA complex. *J. Am. Chem. Soc. 119*, 6711−6721.
(29) Corneliscu, G., Delaglio, F., and Bax, A. (1999) Protein backbone angle restraints from searching a database for chemical shift and sequence homology. *J. Biomol. NMR 13*, 289−302.
(30) Herrmann, T., Guntert, P., and Wuthrich, K. (2002) Protein NMR structure determination with automated NOE-identification in the NOESY spectra using the new software ATNOS. *J. Biomol. NMR 24*, 171−189.
(31) Herrmann, T., Guntert, P., and Wuthrich, K. (2002) Protein NMR structure determination with automated NOE assignment using the new software CANDID and the torsion angle dynamics algorithm DYANA. *J. Mol. Biol. 319*, 209−227.
(32) Schwieters, C. D., Kuszewski, J. J., Tjandra, N., and Clore, G. M. (2003) The Xplor-NIH NMR molecular structure determination package. *J. Magn. Reson. 160*, 65−73.
(33) Karpishin, T. B., and Raymond, K. N. (1992) The first structural characterization of a metal−enterobactin complex: $[V(enterobactin)]^{2-}$. *Angew. Chem., Int. Ed. Engl. 31*, 466−468.
(34) Schuettelkopf, A. W., and van Aalten, D. M. F. (2004) PRODRG: a tool for high-throughput crystallography of protein-ligand complexes. *Acta Crystallogr., Sect. D 60*, 1355−1363.
(35) Eichmuller, C., Schuler, W., Konrat, R., and Krautler, B. (2001) Simultaneous measurement of intra- and intermolecular NOEs in differentially labeled protein-ligand complexes. *J. Biomol. NMR 21*, 107−116.
(36) Bath, J. L., Robinson, M., Kennedy, M. W., Agbasi, C., Linz, L., Maetzold, E., Scheidt, M., Knox, M., Ram, D., Hein, J., Clark, C., and Drees, J. (2009) Identification of a secreted fatty acid and retinol-binding protein (Hp-FAR-1) from *Heligmosomoides polygyrus*. *J. Nemat. 41*, 228−233.
(37) Angelucci, F., Johnson, K. A., Baiocco, P., Miele, A. E., Brunori, M., Valle, C., Vigorosi, F., Troiani, A. R., Liberti, P., Cioli, D., Klinkert, M. Q., and Bellelli, A. (2004) *Schistosoma mansoni* fatty acid binding protein: specificity and functional control as revealed by crystallographic structure. *Biochemistry 43*, 13000−13011.
(38) Balendiran, G. K., Schnutgen, F., Scapin, G., Borchers, T., Xhong, N., Lim, K., Godbout, R., Spener, F., and Sacchettini, J. C. (2000) Crystal structure and thermodynamic analysis of human brain fatty acid-binding protein. *J. Biol. Chem. 275*, 27045−27054.
(39) Shimamoto, S., Yoshida, T., Inui, T., Gohda, K., Kobayashi, Y., Fujimori, K., Tsurumura, T., Aritake, K., Urade, Y., and Ohkubo, T. (2007) NMR solution structure of lipocalin-type prostaglandin D synthase: evidence for partial overlapping of catalytic pocket and retinoic acid-binding pocket within the central cavity. *J. Biol. Chem. 282*, 31373−31379.
(40) Eichinger, A., Nasreen, A., Kim, H. J., and Skerra, A. (2007) Structural insight into the dual ligand specificity and mode of high density lipoprotein association of apolipoprotein D. *J. Biol. Chem. 282*, 31068−31075.
(41) Paesen, G. C., Adams, P. L., Nuttall, P. A., and Stuart, D. L. (2000) Tick histamine-binding proteins: lipocalins with a second binding cavity. *Biochim. Biophys. Acta 1482*, 92−101.
(42) Clifton, M. C., Corrent, C., and Strong, R. K. (2009) Siderocalins: siderophore-binding proteins of the innate immune system. *Biometals 22*, 557−564.